Journal Pre-proofs

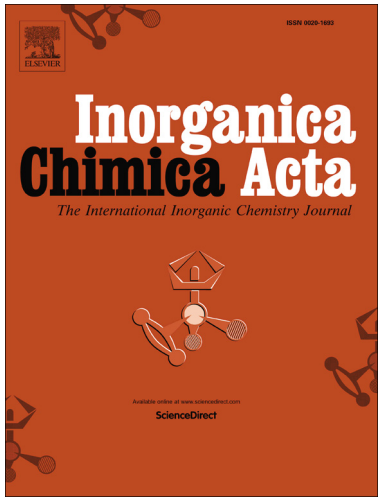

Research paper

Bioinspired Iron(II)-β-Diketonate and Iron(II)-α-Hydroxy Ketone Complexes of a Carbanionic N3C Ligand: Oxidation of Metal Center vs C-C Bond Cleavage of Co-ligand with Dioxygen

Sridhar Banerjee, Tapan Kanti Paine

PII: S0020-1693(19)31195-8
DOI: https://doi.org/10.1016/j.ica.2019.119200
Reference: ICA 119200

To appear in: *Inorganica Chimica Acta*

Received Date: 13 August 2019
Revised Date: 7 October 2019
Accepted Date: 7 October 2019

Please cite this article as: S. Banerjee, T.K. Paine, Bioinspired Iron(II)-β-Diketonate and Iron(II)-α-Hydroxy Ketone Complexes of a Carbanionic N3C Ligand: Oxidation of Metal Center vs C-C Bond Cleavage of Co-ligand with Dioxygen, *Inorganica Chimica Acta* (2019), doi: https://doi.org/10.1016/j.ica.2019.119200

Bioinspired Iron(II)-β-Diketonate and Iron(II)-α-Hydroxy Ketone Complexes of a Carbanionic N3C Ligand: Oxidation of Metal Center vs C-C Bond Cleavage of Co-ligand with Dioxygen

*Sridhar Banerjee and Tapan Kanti Paine**

School of Chemical Sciences, Indian Association for the Cultivation of Science,

2A & 2B Raja S. C. Mullick Road, Jadavpur, Kolkata 700032, India

Fax: +91-33-2473-2805; Tel: +91-33-2473-4971

Abstract

Two bioinspired low-spin iron(II)-ß-diketonate complexes, $[(L^1)Fe^{II}(BA)]$ (**2**) and $[(L^1)Fe^{II}(DBM)]$ (**3**), and an iron(II)-α-hydroxy ketone complex $[(L^1)Fe^{II}(HAP)]$ (**4**) (L^1 = tris(2-pyridylthio)methanido anion, BA = monoanionic benzoylacetone, DBM = monoanionic dibenzoylmethane and HAP = monoanionic 2-hydroxyacetophenone) of a tripodal carbanionic ligand were prepared from an iron(II) precursor complex $[(L^1)Fe^{II}(CH_3CN)_2](ClO_4)$ (**1**). The dioxygen reactivity of the complexes (**2**, **3** and **4**) was investigated to evaluate the effect of ligand geometry and of the spin state of iron on the C-C bond cleavage of the co-ligands. Complexes **2** and **3** react with dioxygen to yield benzoic acid as a minor product. The major pathway involves the formation of the corresponding iron(III)-β-diketonate complexes, $[(L^1)Fe^{III}(BA)](ClO_4)$ (**2^{ox}-ClO_4**) and $[(L^1)Fe^{III}(DBM)](ClO_4)$ (**3^{ox}-ClO_4**). Complex **4**, however, undergoes the C-C bond cleavage of the iron-coodinated HAP to form benzoic acid as the major product. In the reaction, phenylglyoxal is formed as the minor product with concomitant generation of an iron-oxygen oxidant. The oxidant is able to transfer an oxygen atom to thioanisole and can exchange its oxygen atom with water. The reactivity patterns of the low-spin iron(II) complexes reported here are distinctly different from that of the corresponding high-spin complexes supported by a monoanionic facial N3 ligand. The results emphasize the role of spin-state of iron, the denticity of the supporting ligand, and the nature of co-ligand in affecting the C-C bond cleavage reaction.

Keywords: iron complex; carbanionic ligand; dioxygen; oxidation; aliphatic C-C cleavage

1. Introduction

The oxidative cleavage of aliphatic C-C bonds is often a key step in the biodegradation process of toxic chemicals by microorganisms.[1] Aerobic bacteria employ a range of metalloenzymes to carry out the biodegradation process by using molecular oxygen as the terminal electron acceptor.[2, 3] Acetylacetone dioxygenase (Dke1) from *Acinetobacter johnsonii* is one such nonheme enzyme involved in the degradation of acetylacetone, a toxic chemical frequently used in chemical industries (Scheme 1).[4-6] In the process, acetylacetone is oxidatively cleaved to form one equivalent of carboxylic acid and one equivalent of pyruvaldehyde with the incorporation of one oxygen atom into each product. The enzyme is also capable of cleaving the C-C bond other β-diketones.[7] 2,4'-Dihydroxyacetophenone dioxygenase (DAD) from *Alcaligenes sp.*, another nonheme iron enzyme, is involved in the aliphatic C-C bond cleavage of 2,4'-dihydroxyacetophenone to yield 4-hydroxy benzoate using dioxygen as the oxidant (Scheme 1).[8-12] In spite of the differences in activities, these two enzymes (Dke1 and DAD) share some common features. Both belong to the cupin superfamily of enzymes with the active site iron(II) center coordinated by three histidine residues.[13-15]

Over the last couple of decades, attempts have been made to develop functional models of these enzymes. These model studies provide mechanistic information about the C-C cleavage pathways. Though structural models of Dke1 were available in the early 1990s,[16] the first functional model was developed in 2008.[17] Subsequently, a number of studies established that electron-rich substrates were necessary to trigger the oxygen activation mechanism at the metal centre.[17-20] [21-23] Recently, a series of α-hydroxy ketone complexes of tridentate and tetradentate ligands have been reported as functional models of DAD.[24, 25] With an objective to understand the effect of the spin state of metal ion and the nature of supporting ligand on the C-C bond cleaving reactivity of ß-diketones/α-hydroxy ketones by dioxygen, we have

investigated the reactivity of an iron(II) complex of a tetradentate ligand (tris(2-pyridylthio)methanido; L^1).[26] The anionic ligand coordinates in N_3C mode and provides two labile *cis* coordination sites for substrates or dioxygen. It has been reported that iron–carbon bonding in the iron(II) complexes tune the reactivity toward dioxygen. Moreover, the ligand stabilizes iron(II) in low-spin state.[27-32] We report here the synthesis and characterization of two low-spin iron(II)-ß-diketonate complexes, $[(L^1)Fe^{II}(BA)]$ (**2**) and $[(L^1)Fe^{II}(DBM)]$ (**3**), and a low-spin iron(II)-α-hydroxy ketone complex $[(L^1)Fe^{II}(HAP)]$ (**4**) (BA = monoanionic benzoylacetone, DBM = monoanionic dibenzoylmethane and HAP = monoanionic 2-hydroxyacetophenone). The reactivity of the complexes towards molecular oxygen, the effect of ligand, and the oxidation of substrate vs metal center oxidation are presented in this work.

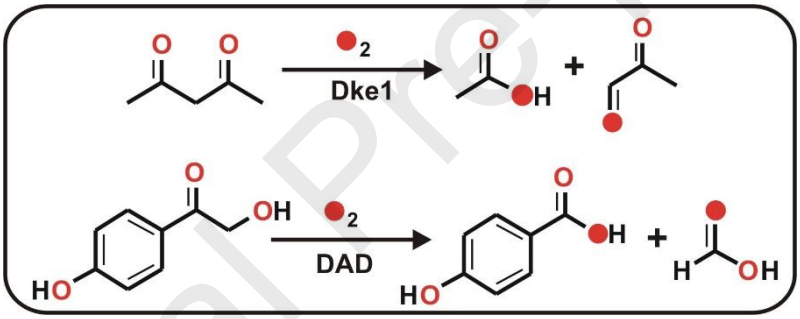

Scheme 1. Biological oxidations catalyzed by Dke1 and DAD.

2. Experimental part

2.1. Materials and methods

All reagents were purchased from commercial sources and were used without further purification, unless otherwise noted. Solvents were distilled, dried and deoxygenated before use. Preparation and handling of air-sensitive materials were carried out under an inert atmosphere in a glove box unless otherwise mentioned. The ligand (HL^1)[26] and the iron(II)-acetonitrile complex (**1**)[29] were prepared following the protocols reported in literature. *Caution: Although*

no problem was encountered during the synthesis of complexes, perchlorate salts are potentially explosive and should be handle with care! [33]

Fourier transform infrared (IR) spectroscopy on KBr pellets was performed on a Shimadzu FT-IR 8400S instrument. Elemental analyses were performed on a PerkinElmer 2400 series II CHN analyser. Electrospray ionisation (ESI) mass spectra were recorded with a Waters QTOF Micro YA263 instrument. Solution electronic spectra (single and time-dependent) were measured on an Agilent 8453 diode array spectrophotometer. Room temperature ^{1}H NMR spectra were collected on a Bruker DPX spectrometer. X-band EPR measurements were performed on a JEOL JES-FA 200 instrument. Cyclic voltammetry was performed by using a PC-controlled PAR (model 273A) electrochemistry system. GC-MS measurements were carried out with PerkinElmer Clarus 680 GC and SQ8T MS instruments, using an Elite 5 MS (30 m × 0.25 mm × 0.25 μm) column with a maximum temperature of 300°C. Labelling experiments were carried out with $^{18}O_2$ gas (99 atom %) purchased from Icon Services Inc., USA or with $H_2{}^{18}O$ (97 atom %) purchased from Sigma-Aldrich.

2.2. Synthesis of complexes

General method for the synthesis of iron(II)-ß-diketonate complexes: β-Diketone (0.25 mmol) was added to an acetonitrile solution (15 mL) of $[(L^1)Fe^{II}(CH_3CN)_2](ClO_4)$ (**1**) (0.15 g, 0.25 mmol) in inert atmosphere. The solution was then treated with triethylamine (35μL, 0.25 mmol) dissolved in acetonitrile (5 mL). The color of the solution changed from red to deep violet. The solvent was then removed under vacuum to isolate a deep violet solid. The crude solid was then washed with diethyl ether and hexane several times to remove any impurity. The deep violet solid was redissolved in dichloromethane and the solution was filtered. The pure complex was isolated by removing the solvent under reduced pressure.

[(L^1)Fe^{II}(BA)] (2): Yield: 0.11 g (79%). Elemental analysis calcd (%) for [(L^1)Fe^{II}(BA)] ($C_{26}H_{21}FeN_3O_2S_3$): C 55.81, H 3.78, N 7.51; Found: C 55.74, H 3.62, N 7.42. IR (KBr): 3460(br), 3056(w), 2960 (w), 2927(m), 1585(s), 1549(s), 1512(s), 1483(m), 1448(vs), 1417(vs), 1274(w), 1145(br, m), 1095(w), 1064(w), 1066(w), 837(w) cm^{-1}. ESI-MS (positive ion mode in CH_3CN): *m/z* (%) 558.9 (100) $[(L^1)Fe(BA)]^+$. ^1H NMR (300 MHz, $CDCl_3$, 25°C): δ, ppm 13.61 (bs), 10.29 (bs), 8.78 (s, 2H), 8.52 (s, 2H), 8.25 (s, H), 7.04 (s, H), 3.48 (s, H), 1.85 (s, H), 1.52 (bs, 2H), 1.22 (m, H), -2.34 (bs). UV-vis-NIR (CH_2Cl_2); λ (ε, $mol^{-1}cm^{-1}$): 540 nm (1800), 480 nm (1660).

[(L^1)Fe^{II}(DBM)] (3): Yield: 0.12 g (77%). Elemental analysis calcd (%) for [(L^1)Fe^{II}(DBM)] ($C_{31}H_{23}FeN_3O_2S_3$): C 59.90, H 3.73, N 6.76; Found: C 59.81, H 3.84, N 6.88. IR (KBr): 3058(w), 1583(m), 1533(s), 1514(vs), 1481(s), 1448(vs), 1417(vs), 1143(m), 1101(w), 756(s) cm^{-1}. ESI-MS (positive ion mode in CH_3CN): *m/z* (%) 620.5 (100) $[(L^1)Fe(DBM)-H]^+$. ^1H NMR (300 MHz, $CDCl_3$, 25°C): δ, ppm: 8.40 (m, 3H), 7.63 (t, J = 7.2 Hz, 2H), 7.45 (m, H), 7.31 (m, 6H), 7.12 (m, 6H), 6.82 (bs, 3H), 6.40 (bs, 2H). UV-vis (CH_2Cl_2); λ (ε, $mol^{-1}cm^{-1}$): 490 nm (2120), 550 nm (2950), 650 nm (1990).

General method for the synthesis of iron(III)-ß-diketonate complexes: Complex **2** and **3** (0.5 mmol) dissolved in acetonitrile (12 mL) was separately treated with an acetonitrile solution of sodium perchlorate (0.12 g, 1 mmol). The purple solution was then exposed to dioxygen and was allowed to stir under oxygen atmosphere for 12 h. The crude solid, obtained upon removal of solvent, was dissolved in dichloromethane and was kept for layer diffusion with hexane to obtain the pure compound. X-ray quality single crystals were grown by the slow layer diffusion of hexane into a dichloromethane solution of the complex.

$[(L^1)Fe^{III}(BA)]ClO_4$ (2^{ox}-ClO_4): Yield: 0.26 g (80%). Elemental analysis calcd (%) for $[(L^1)Fe^{III}(BA)]ClO_4$ ($C_{26}H_{21}ClFeN_3O_6S_3$): C 47.39, H 3.21, N 6.38; Found: C 47.73, H 3.14, N 6.36. IR (KBr): 3439(br), 3101(w), 3066 (w), 2923(w), 1589(s), 1535(vs), 1516(vs), 1487(m), 1454(m), 1421(s), 1309(w), 1280(s), 1086vs), 1194(s), 767(s), 621(m) cm^{-1}. ESI-MS (positive ion mode in CH_3CN): *m/z* (%) 558.9 (100) $[(L^1)Fe(BA)]^+$.

$[(L^1)Fe^{III}(DBM)]ClO_4$ (3^{ox}-ClO_4): Yield: 0.27 g (75%). Elemental analysis calcd (%) for $[(L^1)Fe^{III}(DBM)]ClO_4$ ($C_{31}H_{23}ClFeN_3O_6S_3$): C 51.64, H 3.22, N 5.83; Found: C 51.52, H 3.19, N 5.85. IR (KBr): 3433(br), 3097(w), 3060 (w), 1589(s), 1521(vs), 1481(s), 1452(m), 1421(m), 1325(m), 1280(m), 1081(m), 765(m) cm^{-1}. ESI-MS (positive ion mode in CH_3CN): *m/z* (%) 621.00 (100) $[(L^1)Fe(DBM)]^+$.

Synthesis of $[(L^1)Fe^{II}(HAP)]$ (4): An acetonitrile solution (5 mL) of 2-hydroxyacetophenone (0.034 g, 0.25 mmol) and triethylamine (35 μL) was added to an acetonitrile solution (15 mL) of $[(L^1)Fe^{II}(CH_3CN)_2](ClO_4)$, (**1**) (0.15 g, 0.25 mmol). The resulting solution was allowed to stir for 30 min and then the solvent was removed under reduced pressure. The residue was redissolved in dichloromethane and the solution was filtered. A deep red solid was isolated from the filtrate by removing the solvent. The crude solid was washed several times with diethyl ether to get the pure complex. Yield: 0.10 g (76%). Elemental analysis calcd (%) for $[(L^1)Fe^{II}(HAP)]\cdot CH_2Cl_2$ ($C_{27}H_{21}FeN_3O_2S_3Cl_2$): C 48.56, H 3.42, N 6.79; Found: C 48.03, H 3.82, N 6.40. IR (KBr): 3431 (br), 3415(br), 3058(w), 2924(m), 1587(s), 1541(s), 1514(s), 1483(m), 1448(s), 1421(s), 1280(m), 1145(m), 1089(br), 766(w) cm^{-1}. ESI-MS (positive ion mode in CH_3CN): *m/z* (%) 549.21 (100) $[(L^1)Fe(HAP)(O)]^+$, 508.17 (10) $[(L^1)Fe(PyS)]^+$, 415.15 (40) $[(L^1)Fe(OH)]^+$. ^1H NMR (300 MHz, CD_3CN, 25°C): δ, ppm: 8.80 (br, 2H), 7.91 (m, 2H), 7.82 (d, J =7.9 Hz, 2H),

7.73 (m, H), 7.63 (m, H), 7.51 (dd, *J* = 7.9 Hz, 2H), 7.43 (dd, *J* = 7.5 Hz, 3H), 7.15 (d, *J* = 7.9 Hz, 2H), 7.07 (m, H), 6.91 (t, *J* = 7.3 Hz, 3H), 4.82(s, 2H).

2.3. Oxygenation of the iron(II)-ß-diketonate complexes and analysis of cleavage products:

The complex **(**0.02 mmol; 11.1 mg for **2**, 12.5 mg for **3**) was dissolved in acetonitrile (20 mL). Pure dioxygen was bubbled through the solution and was allowed to stir (2 h for **2**, 12 h for **3**). Then the solvent was removed under vacuum, 10 mL of 3M HCl was added to the residue and allowed to stir for 2 h. The organic products were extracted with diethyl ether (3×15 mL) and the was dried over anhydrous Na_2SO_4. The products were analyzed by ^{1}H NMR spectroscopy.

2.4. Oxygenation of the iron(II)-α-hydroxy ketone complex and analysis of cleavage products:

Complex **4** (10.6 mg, 0.02 mmol) was dissolved in ~20 mL acetonitrile. Pure dioxygen was bubbled through the solution and was allowed to stir for 30 min. Then the solvent was removed under vacuum, 10 mL of 3M HCl was added to the residue and allowed to stir for 2 h. The organic products were extracted with diethyl ether (3×15 mL), dried over anhydrous Na_2SO_4 and the solvent removed under vacuum. The products were analyzed by ^{1}H NMR spectroscopy and GC-mass spectrometry. Benzoic acid obtained from the oxidized solution was treated with excess amount of diazomethane in diethyl ether. The solution was allowed to stir for 5 min and then filtered to get the solution of methylbenzoate as a filtrate.

2.6. X-ray crystallographic data collection, refinement and solution of the structure

Single crystal X-ray data of the complexes were collected using Mo Kα (λ = 0.7107 Å) radiation on a SMART APEX II diffractometer equipped with CCD area detector. Data collection, data reduction, structure solution/refinement were carried out using the software package of APEX II.[34] The structures were solved by direct method and subsequent Fourier analyses and refined by the full-matrix least-squares method based on F^2 with all observed

reflection.[35] Non hydrogen atoms were treated anisotropically and hydrogen atoms were geometrically fixed. The unit cell of **3^{ox}-ClO_4** contained two disordered dichloromethane molecules which were treated as diffuse contribution to overall scatter without specific atom positions using SQUEEZE/PLATON.[36]

3. Results and discussion

The iron(II)-diketonate complexes (**2** and **3**) were prepared from the reactions of the iron(II)-acetonitrile complex (**1**)[29] with respective ß-diketone and a base (Et_3N) in acetonitrile. Complex **4** was isolated from the reaction of **1** with 1 equiv of 2-hydroxyacetophenone and triethylamine in acetonitrile (Scheme 2). The complexes were characterized by IR, ESI-MS, ^{1}H NMR spectroscopy and elemental analysis (Experimental and Figure S1-S6). All the three complexes show strong bands near 1580 cm^{-1}, indicative of coordinated carbonyl group, in their IR spectra. The presence of such band in the IR spectrum of complex **4** suggests that the bidentate binding of HAP in the keto form. The ^{1}H NMR spectra of the complexes are similar to those of the low-spin iron(II) complexes of the same ligand.[28, 29, 31] The spectrum of complex **2** (Figure S4), however, shows resonance signals with slight paramagnetic shifting and line broadening. This may be attributed to the presence of a paramagnetic impurity, which may originate from the oxidation of **2** by oxygen (vide infra) during data collection.

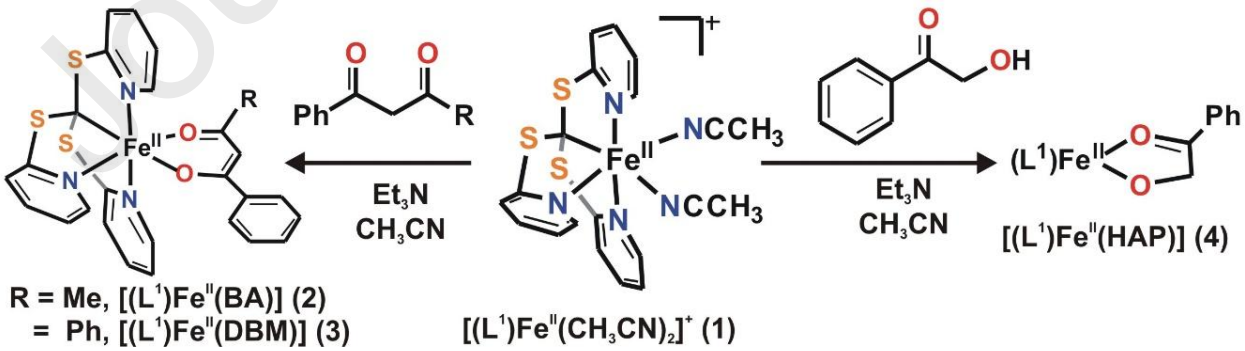

Scheme 2. Synthesis of iron(II) complexes.

Complex **2** shows strong charge-transfer (CT) bands at 480 and 540 nm in the optical spectrum. Likewise, complex **3** shows CT bands at 490, 550 and 650 nm (Figure 1). These CT bands can be attributed to the iron(II)-to-diketonate (MLCT) transitions.[13, 18] However, in case of the α-hydroxy ketone complex **4**, the CT bands are blue shifted (408 and 450 nm) (Figure 1). The LUMO of β-diketonates in **2** and **3** are stabilized due to extended delocalization of π-electrons, which is absent in **4**. Thus, the MLCT bands appear in lower energy in iron(II)-β-diketonate complexes compared to the iron(II)-α-hydroxy ketone complex.

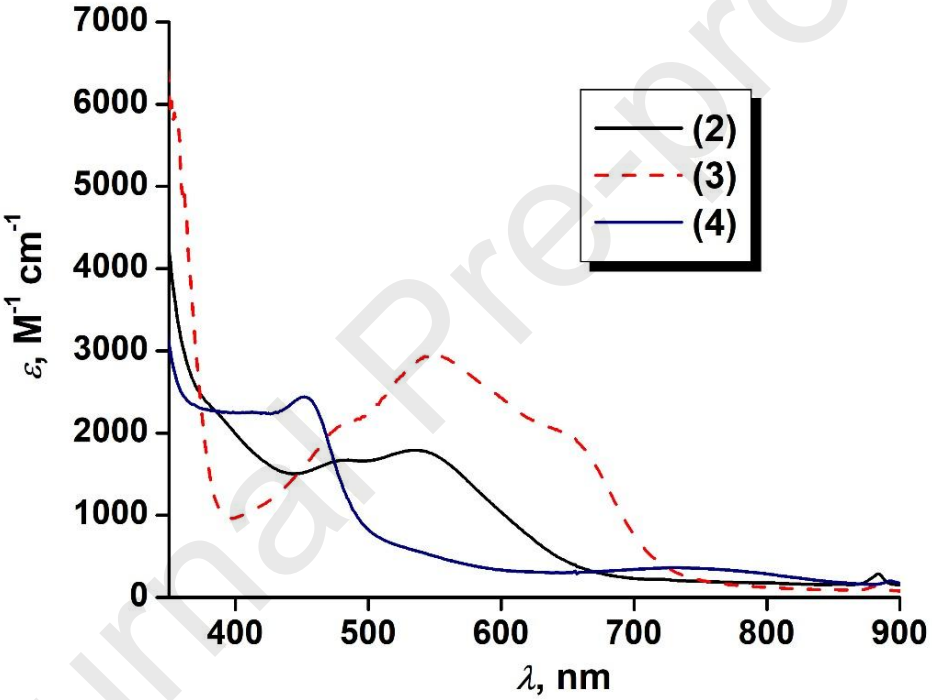

Figure 1. Optical spectra of iron(II)-β-diketonate and iron(II)-α-hydroxy ketone complexes in acetonitrile at 298 K.

To confirm the binding modes of the supporting ligand and the co-ligands, several attempts were made to isolate single crystals of the complexes. All attempts to crystalize complexes **2** and **4** failed. However, X-ray quality single crystals of complex **3** were obtained by slow diffusion of diethyl ether into the solution of the complex in dichloromethane (Table S1).

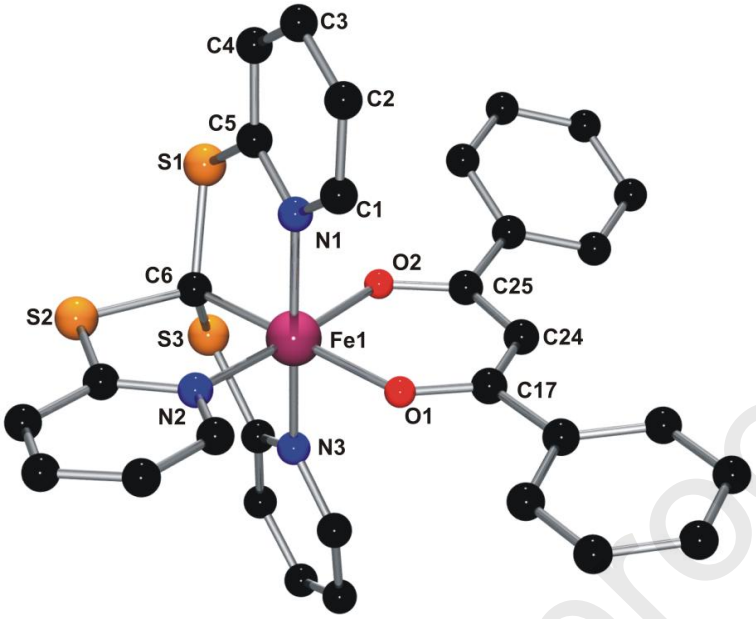

Figure 2. Molecular structure of the neutral complex [(L^1)Fe^{II}(DBM)] (**3**).

The crystal structure of **3** shows a six-coordinate iron(II) centre ligated by three pyridine nitrogens (N1, N2 and N3) and one anionic carbon (C6) from the ligand (L^1) and two oxygen donors (O1 and O2) from dibenzoylmethane (DBM) (Figure 2). A strong iron(II)-carbon bonding interaction with the Fe1–C6 distance of 1.955(16) Å is observed (Table 1). The average Fe–N bond distance of 1.969 Å is comparable to that reported for low-spin iron(II) complexes of the N_3C ligand.[27-29, 31] In the distorted octahedral geometry, the anionic DBM binds to the iron center in a chelating bidentate fashion resulting in a six-membered chelate ring. The C(17)-O(1) and C(25)-O(2) bonds, and the C(17)-C(24) and C(24)-C(25) bonds of DBM display very similar distances (within standard deviations) confirm enolization upon coordination with the iron center. As a result, two oxygens and three carbons of the enolate constitute a plane. One of the phenyl rings of DBM shows a deviation of 25.77° from the enolate plane, whereas the other phenyl ring is oriented at an angle of 8.88° with respect to the enolate plane. The Fe-$O_{enolate}$ bond

(Fe1-O1 distance of 1.979 Å) trans to the strong Fe1-C6 bond is elongated compared to the Fe1-O2 bond (1.936 Å).

Reactivity of the iron(II)-β-diketonate complexes toward dioxygen

The deep violet acetonitrile solution of **2** reacts with dioxygen under ambient conditions to form a green solution. During the reaction, the CT bands at 540 nm and 480 nm disappear within 30 min (k_{obs} =7.8 x 10^{-4} s^{-1}) indicating the oxidation of the complex (Figure 3). The reaction of complex **3** with dioxygen, however, takes place at a much slower rate. In the reaction, the metal to ligand charge-transfer bands at 490 nm, 550 nm and 650 nm slowly decay over a period of 12 h (Figure S7). The organic products from β-diketones after the reaction with dioxygen were identified and quantified by ^{1}H NMR spectroscopy (Figure S8). In both the cases, benzoic acid is formed, and the yields are calculated to be 11% and 13% for **2** and **3**, respectively. Thus, a small percentage of β-diketone undergoes C-C bond cleavage pathway.

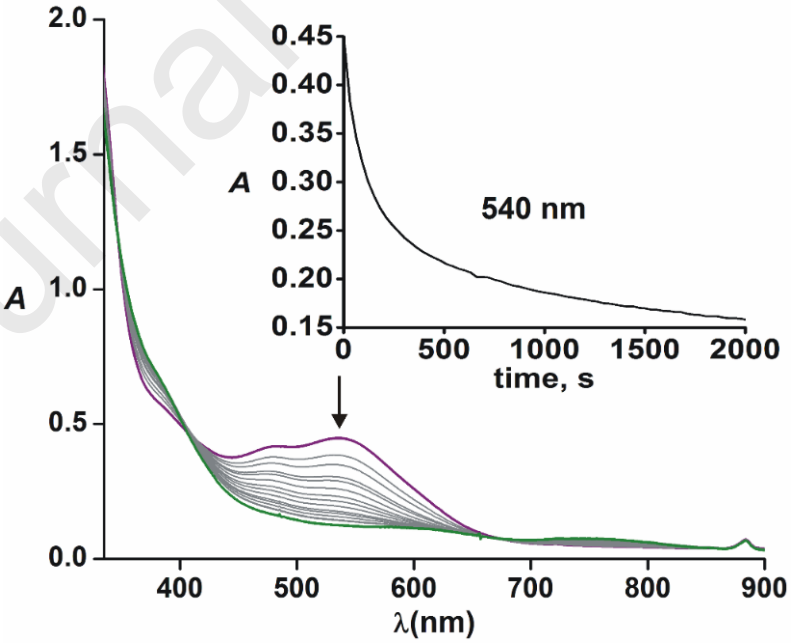

Figure 3. UV-vis spectral changes of complex **2** (0.25 mM) in acetonitrile upon exposure to dioxygen at 298 K.

To assess the fate of the iron complex in the major pathway, the final oxidized complexes were isolated in solid form with 80% and 75% yield for $\mathbf{2^{ox}\text{-}ClO_4}$ and $\mathbf{3^{ox}\text{-}ClO_4}$, respectively (Experimental section). Both the oxidized complexes display rhombic signals in the X-band EPR spectra (Figures 4a and 4b). The g values confirm the low-spin nature of the iron(III) complexes. Cyclic voltammogram (vs Fc/Fc^{+}) of each of $\mathbf{2^{ox}\text{-}ClO_4}$ and $\mathbf{3^{ox}\text{-}ClO_4}$ in acetonitrile shows a single quasi-reversible redox process ($E_{1/2}$ = -0.713 V for $\mathbf{2^{ox}\text{-}ClO_4}$ and -0.634 V for $\mathbf{3^{ox}\text{-}ClO_4}$) corresponding to the reduction of Fe(III) to Fe(II) species (Figure 4c and 4d).

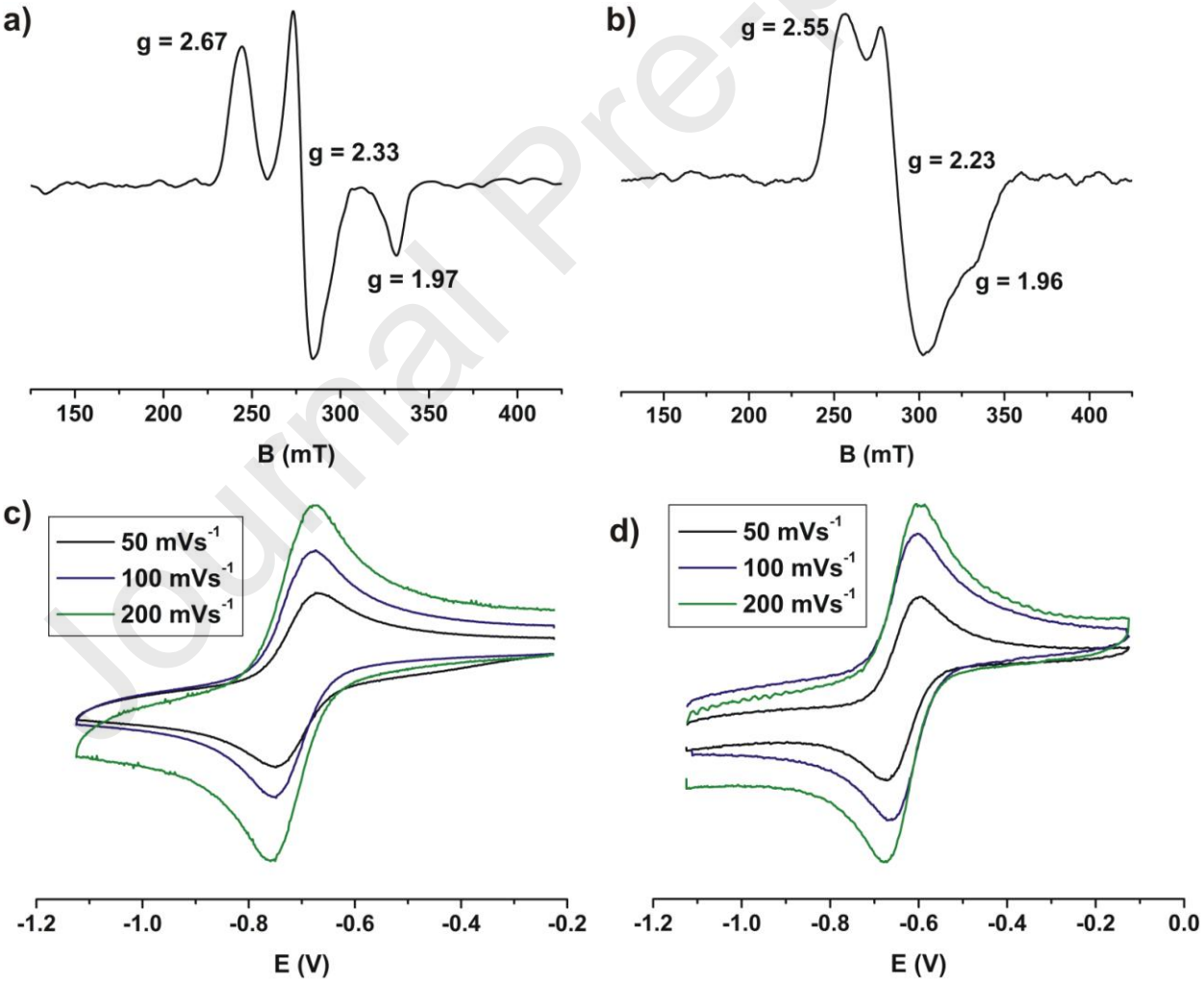

Figure 4. X-band EPR spectra of (a) **2^{ox}-ClO_4** and (b) **3^{ox}-ClO_4**. (Experimental condition: temperature = 77K, microwave frequency = 9.127 GHz, microwave power = 0.998 mW, modulation amplitude = 100 kHz, time constant = 0.03 s, modulation width = 0.7 mT for (a) and 0.1 mT for (b)). Cyclic voltammograms of (c) **2^{ox}-ClO_4** and (d) **3^{ox}-ClO_4** in acetonitrile with different scan rates (0.05–0.2 Vs^{-1}).

X-ray quality single crystals of **2^{ox}-ClO_4** and **3^{ox}-ClO_4** were grown by layer diffusion of hexane into the dichloromethane solution of the respective species. The complex **2^{ox}-ClO_4** crystallized in the *P21/c* space group whereas **3^{ox}-ClO_4** crystallized in the triclinic P-1 space group (Table S1).

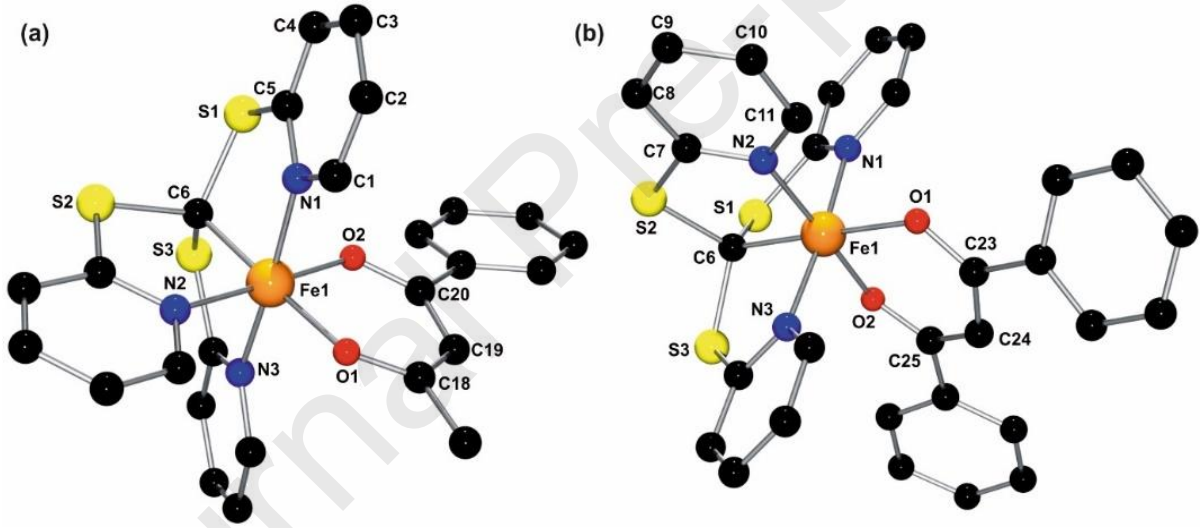

Figure 5. Crystal structure of the complex cation of (a) $[(L^{1})Fe^{III}(BA)](ClO_4)$ (**2^{ox}-ClO_4**) and (b)$[(L^{1})Fe^{III}(DBM)](ClO_4)$ (**3^{ox}-ClO_4**).

The crystal structures **2^{ox}-ClO_4** and **3^{ox}-ClO_4** confirm the N_3CO_2 coordination environment at the iron center of both the complexes (Figures 5a and 5b). While the average Fe–N distance (1.965 Å for **2^{ox}-ClO_4** and 1.973 Å for **3^{ox}-ClO_4**) is comparable to that of the reported low-spin iron(III) complexes of the N_3C ligand,[29, 31] but is not very different from the iron(II)-

diketonate complex **3** (Tables 1-3). The Fe-$O_{diketonate}$ bonds become stronger in the oxidized complexes due to increased Lewis acidity of the metal center. The strong Fe-O bonds in turn forces the iron-carbon bond to elongate slightly. Furthermore, the six-membered chelate ring, formed by the two oxygen atoms and three carbon atoms of β-diketonate at iron center, deviates from planarity in the oxidized complexes compared to that in **3** (Figures 5a and 5b).

Reactivity of the α-hydroxy ketone complex toward dioxygen

Complex **4** reacts with dioxygen in acetonitrile within 15 min, during which the charge transfer band at 450 nm decay pseudo-first-order kinetics (k_{obs} = 4.5 x 10^{-3} s^{-1} at 298 K) (Figure 6). The organic products, extracted from the oxidized solution of **4** with diethyl ether after acid work up, were analysed by ^{1}H NMR spectroscopy (Figure S9). The ^{1}H NMR spectrum reveals the formation of benzoic acid in 62% yield upon oxidative C-C bond cleavage 2-hydroxyacetophenone. The rest 38% of 2-hydroxyacetophenone undergo two-electron oxidation to form the corresponding 1,2-diketone product i.e. phenylglyoxal.

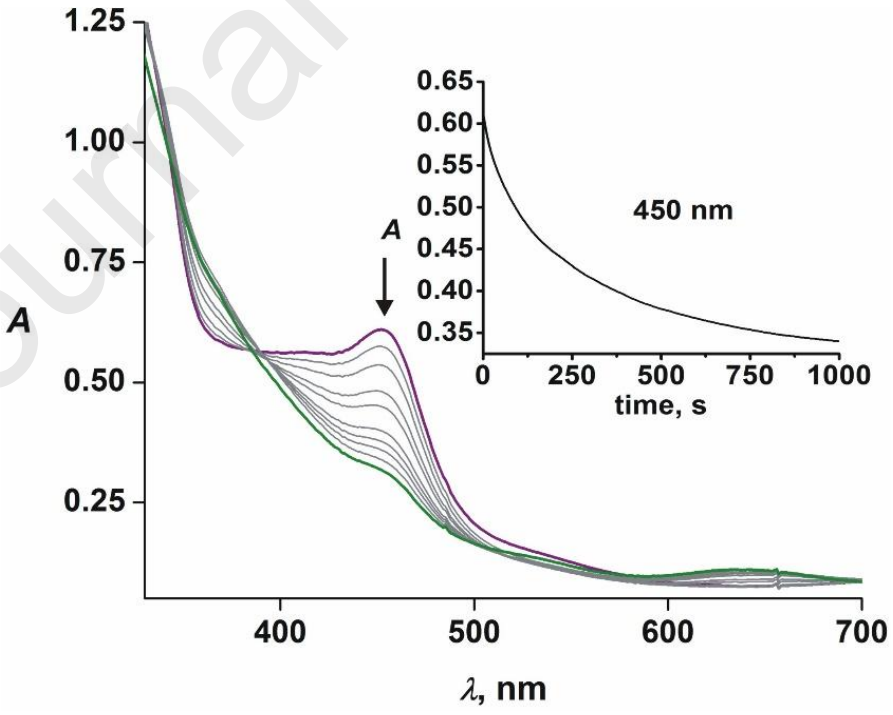

Figure 6. UV-vis spectral changes of complex **4** (0.25 mM) in acetonitrile upon exposure to dioxygen at 298 K.

The formation of benzoic acid was further confirmed by GC-MS analysis (Figure 7a and Figure S10). The GC-mass spectrum of methyl benzoate, prepared from benzoic acid upon treatment with diazomethane, shows an ion peak at *m/z* 136. When the reaction of **4** is carried out with $^{18}O_2$, an additional ion peak is observed at *m/z* 138 (Figure 7b). This result confirms that one oxygen atom from the dioxygen is incorporated into the C-C bond cleavage product. The low percentage of ^{18}O incorporation (~20%) is likely due to some loss by exchange of ^{18}O with water in the reaction pathway or during esterification.[25]

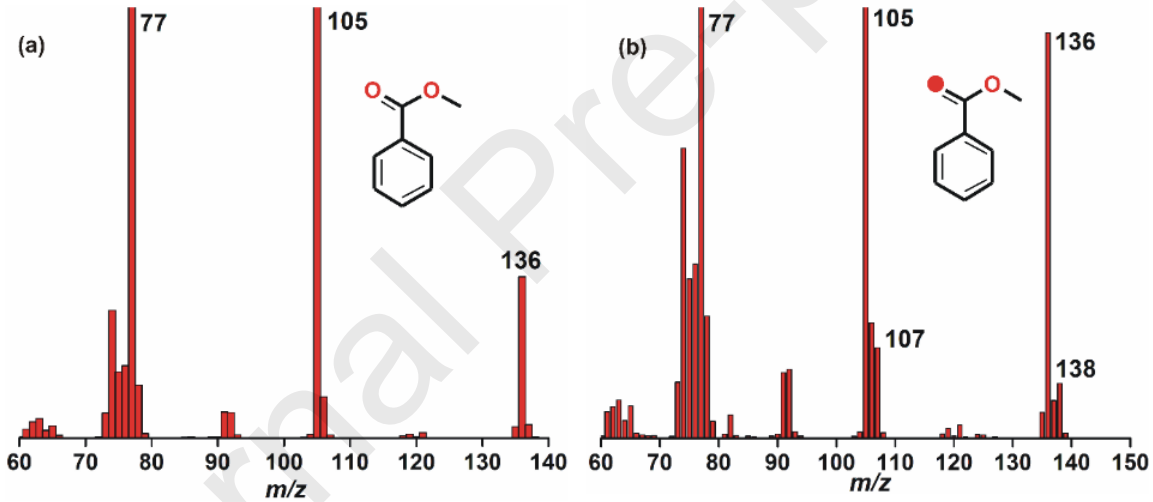

Figure 7. GC-mass spectra of methyl benzoate derived from benzoic acid formed in the reaction of complex **4** with (a) $^{16}O_2$ and (b) $^{18}O_2$.

The molecular ion peak for phenylglyoxal is observed at *m/z* 134, which does not shift when the reaction is performed with $^{18}O_2$ (Figure S10). Therefore, the 1,2-diketone product is not formed in the oxygenation pathway. It is rather formed in the two-electron oxidation of HAP. The electrons from HAP are utilized for the reductive activation of dioxygen on the iron centre to produce an iron-oxygen oxidant. The oxidant thus generated was intercepted by thioanisole.[37]

Of note, the presence of thioanisole does not alter the ratio of benzoic acid and phenylglyoxal confirming that the C-C bond cleavage and the two-electron oxidation of 2-hydroxyacetophenone take place via two independent pathways. The formation of thioanisole oxide (27%) in the interception reaction supports the generation of an iron-oxygen oxidant upon reduction of dioxygen on the iron center.[25] Furthermore, in the oxidation of thioanisole by **4** in the presence of $H_2{}^{18}O$ (5 equiv.), about 20% incorporation of labelled oxygen atom is observed (Figure 8). The result of labelling experiment indicates that the iron-oxygen oxidant can exchange its oxygen atom with water, and for that, the O-O bond has to cleave to generate an iron-oxo species.[38] However, no such species was observed in the reaction pathway and further investigations are required to unravel the nature of the oxidant.

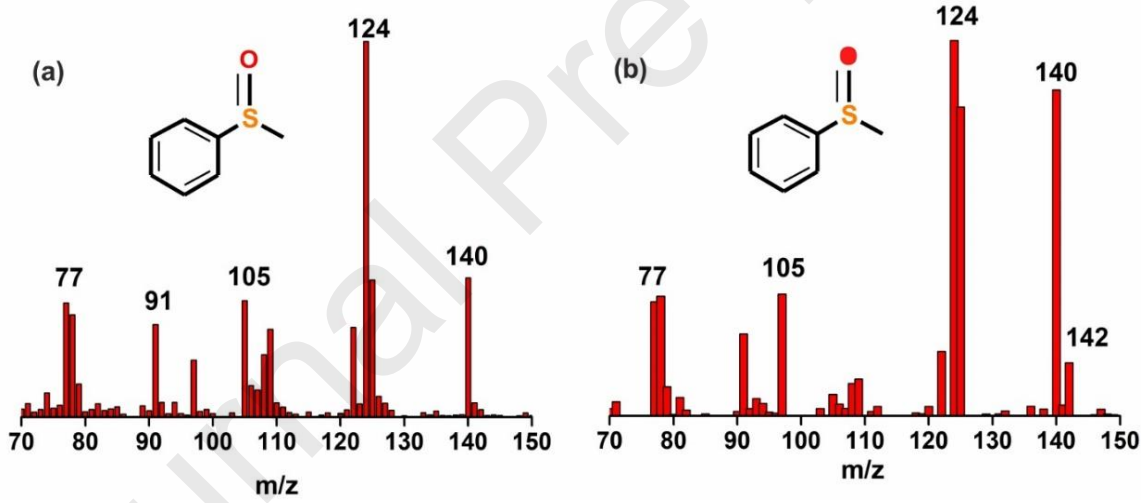

Figure 8. GC-mass spectra of thioanisole oxide formed during the reaction of complex **4** with thioanisole in the presence of (a) $^{16}O_2$ and (b) $^{16}O_2 + H_2{}^{18}O$.

The different reactivity patterns of the iron(II)-β-diketonate and iron(II)-α-hydroxy ketone complexes can be explained in the light of structural and electronic factors. In the iron(II)-β diketonate complexes, the iron centres along with two oxygen atoms and three carbon atoms from the diketonate moiety constitute stable a six-membered ring. The negative charge of the

metal-coordinated enolate can delocalize over the five-membered O-C-C-C-O unit giving extra stabilization of the complexes. Moreover, the lability of metal-ligand bonds in low-spin complexes are less compared to those in high-spin complexes. The six-coordinate stable complexes (**2** and **3**) do not undergo initial ligand dissociation for dioxygen activation at the iron center. For α-hydroxy ketone, on the other hand, a non-planar five-membered chelate ring is formed at the iron center. Thus, it loses resonance stabilization and prefers to undergo oxidative C-C bond cleavage upon dioxygen activation in the major pathway (Scheme 3). While the high-spin iron(II)-α-hydroxy ketone complexes of the facial N3 ligand (Tp^{Ph2} = hydrotris(3.5-diphenylpyrazol-1-yl)borate) have been reported to afford exclusively C-C cleavage products, those of the neutral N4 ligands displayed the C-C cleavage along with two-electron oxidations of α-hydroxy ketones.[24,25] Although the anionic ligand in the low-spin iron(II)-HAP complex (**4**) makes it to react faster with dioxygen, the reactivity is similar to that of the high-spin six-coordinate iron(II)-α-hydroxy ketone complexes of neutral N4 ligands. The C-C cleavage pathway, however, follow a very similar mechanism reported earlier.[25]

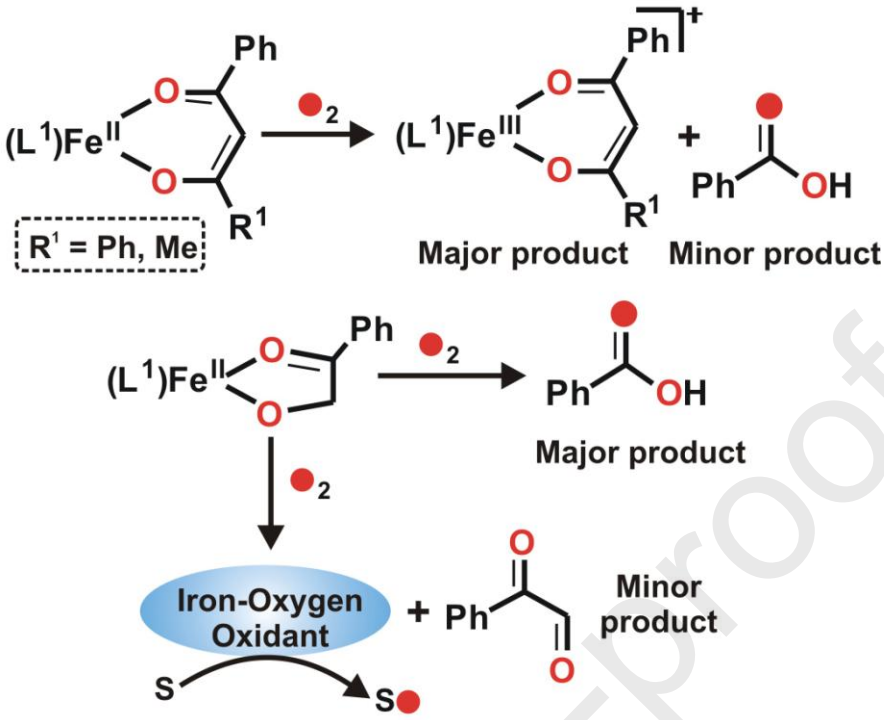

Scheme 3. Reactivity of the iron(II)-ß-diketonate and iron(II)-αhydroxy ketone complexes.

4. Conclusions

We have prepared two iron(II)-β-diketonate complexes and an iron(II)-α-hydroxy ketone complex of a carbanionic N_3C donor ligand. The iron(II)-β-diketonate complexes react with dioxygen and produce the corresponding six-coordinate iron(III) complex as the major product and a small percentage of C-C cleavage product. On the contrary, the iron(II)-α-hydroxy ketone complex displays oxidative C-C cleavage of the co-ligand in the major pathway mimicking the activity of DAD. In a parallel pathway, the α-hydroxy ketone undergoes two-electron oxidation. In the two-oxidation of 2-hydroxyacetophenone, an iron-oxygen oxidant is generated which is able to transfer an oxygen atom to thioanisole and can exchange its oxygen atom with water. Furthermore, the reactivity of the low-spin iron(II)-α-hydroxy ketone complex reported here distinct itself from that of the high-spin complexes supported by a monoanionic N3 ligand.

Compared to the lability of the high-spin complexes, the inert character of the low-spin complex likely explains the difference in reactivity. Furthermore, the reactivity patterns of the biomimetic complexes discussed in this work highlight the role of high-spin metal center with the facial N3 binding motif in the aliphatic C-C bond cleavage reactions catalysed by the nonheme iron enzymes, Dke1and DAD.

Supplementary Material. Spectral and crystallographic data. CCDC 1900628, 1900629 and 1900630 contain the supplementary crystallographic data for **3**, **3^{ox}-ClO_4** and **2^{ox}-ClO_4**, respectively. These data can be obtained free of charge via www.ccdc.cam.ac.uk/data_request/cif or by emailing data_request@ccdc.cam.ac.uk, or by contacting The Cambridge Crystallographic Data Centre, 12, Union Road, Cambridge CB2 1EZ, UK; fax: +44 1223 336033.

Acknowledgments

TKP gratefully acknowledges the Council of Scientific and Insudtrial Reserach (CSIR), India for the financial support (Project No. 01(2926)/18/EMR-II). SB thanks CSIR for a research fellowship.

References

[1] D.T. Gibson, in Microbial Degradation of Organic Compounds, Marcel Dekker, New York, 1984.

[2] S. Fetzner, Appl. Environ. Microbiol., 78 (2012) 2505-2514.

[3] C.J. Allpress, L.M. Berreau, Coord. Chem. Rev., 257 (2013) 3005-3029.

[4] G.D. Straganz, A. Glieder, L. Brecker, D.W. Ribbons, W. Steiner, Biochem J., 369 (2003) 573-581.

[5] G.D. Straganz, S. Egger, G. Aquino, S. D'Auria, B. Nidetzky, J. Mol. Catal. B; Enzymatic, 39 (2006) 171-178.

[6] G.D. Straganz, A.R. Diebold, S. Egger, B. Nidetzky, E.I. Solomon, Biochemistry, 49 (2010) 996-1004.

[7] G.D. Straganz, H. Hofer, W. Steiner, B. Nidetzky, J. Am. Chem. Soc., 126 (2004) 12202-12203.

[8] D.J. Hopper, E.A. Elmorsi, Biochem. J., 218 (1984) 269-272.

[9] D.J. Hopper, H.G. Jones, E. Elmorsi, M.E. Rhodes-Roberts, J. Gen. Microbiol., 131 (1985) 1807-1814.

[10] D.J. Hopper, Biochem. J., 239 (1986) 469-472.

[11] D.J. Hopper, M.A. Kaderbhai, Biochem. J., 344 (1999) 397-402.

[12] A. Tanner, D.J. Hopper, J. Bacteriol., 182 (2000) 6565-6569.

[13] A.R. Diebold, M.L. Neidig, G.R. Moran, G.D. Straganz, E.I. Solomon, Biochemistry, 49 (2010) 6945-6952.

[14] S. Leitgeb, G.D. Straganz, B. Nidetzky, Biochem. J., 418 (2009) 403-411.

[15] R. Keegan, A. Lebedev, P. Erskine, J. Guo, S.P. Wood, D.J. Hopper, S.E.J. Rigby, J.B. Cooper, Acta Cryst., D70 (2014) 2444-2454.

[16] N. Kitajima, H. Amagai, N. Tamura, M. Ito, Y. Moro-oka, K. Heerwegh, A. Penicaud, R. Mathur, C.A. Reed, P.D.W. Boyd, Inorg. Chem., 32 (1993) 3583-3584.

[17] I. Siewert, C. Limberg, Angew. Chem. Int. Ed., 47 (2008) 7953-7956.

[18] H. Park, J.S. Baus, S.V. Lindeman, A.T. Fiedler, Inorg. Chem., 50 (2011) 11978-11989.

[19] H. Park, M.M. Bittner, J.S. Baus, S.V. Lindeman, A.T. Fiedler, Inorg. Chem., 51 (2012) 10279-10289.

[20] M. Sallmann, C. Limberg, Acc. Chem. Res., 48 (2015) 2734-2743.

[21] S. Hoof, M. Sallmann, C. Herwig, B. Braun-Culaa, C. Limberg, Dalton Trans., 46 (2017) 16792-16795.

[22] R. Ramasubramanian, K. Anandababu, M. Kumar, R. Mayilmurugan, Dalton Trans., 47 (2018) 4049-4053.

[23] C.J. Allpress, A. Miłaczewska, T. Borowski, J.R. Bennett, D.L. Tierney, A.M. Arif, L.M. Berreau, J. Am. Chem. Soc., 136 (2014) 7821-7824.

[24] S. Paria, P. Halder, T.K. Paine, Angew. Chem. Int. Ed., 51 (2012) 6195-6199.

[25] R. Rahaman, S. Paria, T.K. Paine, Inorg. Chem., 54 (2015) 10576-10586.

[26] V.D. de Castro, G.M. de Lima, C.A.L. Filgueiras, M.T.P. Gambardella, J. Mol. Str., 609 (2002) 199-203.

[27] P. Halder, A. Dey, T.K. Paine, Inorg. Chem., 48 (2009) 11501-11503.

[28] P. Halder, T.K. Paine, Inorg. Chem., 50 (2011) 708-710.

[29] P. Halder, S. Paria, T.K. Paine, Chem. Eur. J., 18 (2012) 11778-11787.

[30] N. Kuwamura, R. Kato, K.i. Kitano, M. Hirotsu, T. Nishioka, H. Hashimoto, I. Kinoshita, Dalton Trans., 39 (2010) 9988-9993.

[31] S. Banerjee, P. Halder, T.K. Paine, Z. Anorg. Allg. Chem., 640 (2014) 1168-1176.

[32] R. Santo, R. Miyamoto, R. Tanaka, T. Nishioka, K. Sato, K. Toyota, M. Obata, S. Yano, I. Kinoshita, A. Ichimura, T. Takui, Angew. Chem. Int. Ed., 45 (2006) 7611-7614.

[33] W.C. Wolsey, J. Chem. Educ., 50 (1973) A335-A337.

[34] APEX 2, version 2.1-0; Bruker AXS; Madison, WI, 2006.

[35] G.M. Sheldrick, SHELXL-97, Program for crystal structure refinement, University of Göttingen, Göttingen, Germany, 1997.

[36] A.L. Spek, PLATON. A multipurpose crystallographic tool, Utrecht University, Utrecht, The Netherlands, 2002.

[37] A. Mukherjee, M. Martinho, E.L. Bominaar, E. Münck, L. Que, Jr., Angew. Chem. Int. Ed., 48 (2009) 1780-1783.

[38] M. S. Seo, J. In, S. O. Kim, N. Y. Oh, J. Hong, J. Kim, L. Que, Jr., W. Nam, Angew. Chem. Int. Ed., 43 (2004) 2417-2420.

Table 1. Selected bond lengths (Å) and angles (°) for [(L^{I})Fe^{II}(DBM)] (**3**).

Fe(1)–N(1)	1.959(15)	Fe(1)–N(2)	1.971(14)
Fe(1)–N(3)	1.977(15)	Fe(1)–C(6)	1.955(16)
Fe(1)–O(1)	1.979(11)	Fe(1)–O(2)	1.936(11)
C(25)–O(2)	1.269(2)	C(17)–O(1)	1.277(19)
C(17)–C(24)	1.397(2)	C(24)–C(25)	1.400(2)
C(6)–Fe(1)–N(1)	87.94(7)	C(6)–Fe(1)–O(1)	179.16(7)
N(1)–Fe(1)–N(2)	91.05(6)	C(6)–Fe(1)–N(3)	87.83(7)

O(1)–Fe(1)–O(2)	91.99(5)	N(2)–Fe(1)–N(3)	94.54(6)
C(6)–Fe(1)–N(2)	89.15(6)	N(3)–Fe(1)–N(1)	172.93(6)
N(1)–Fe(1)–O(1)	92.85(6)	N(1)–Fe(1)–O(2)	86.90(6)
O(2)–Fe(1)–C(6)	87.77(6)	N(3)–Fe(1)–O(1)	91.36(6)
N(2)–Fe(1)–O(2)	176.35(6)	N(3)–Fe(1)–O(2)	87.29(6)
N(2)–Fe(1)–O(1)	91.13(5)		

Table 2. Selected bond lengths (Å) and angles (°) for $[(L^{1})Fe^{III}(BA)](ClO_4)\cdot CH_2Cl_2$ (**2^{ox}-ClO_4**).

Fe(1)–N(1)	1.959(5)	Fe(1)–N(2)	1.975(5)
Fe(1)–N(3)	1.962(5)	Fe(1)–C(6)	1.979(6)
Fe(1)–O(1)	1.922(4)	Fe(1)–O(2)	1.901(4)
C(20)–O(2)	1.272(7)	C(18)–O(1)	1.296(7)
C(6)–Fe(1)–N(1)	85.4(2)	C(6)–Fe(1)–O(1)	178.3(2)
N(1)–Fe(1)–N(2)	92.2(2)	C(6)–Fe(1)–N(3)	87.2(2)
O(1)–Fe(1)–O(2)	92.03(17)	N(2)–Fe(1)–N(3)	88.8(2)
C(1)–Fe(1)–N(2)	90.8(2)	N(3)–Fe(1)–N(1)	172.5(2)
N(1)–Fe(1)–O(1)	93.17(19)	N(1)–Fe(1)–O(2)	89.61(19)
O(2)–Fe(1)–C(6)	88.8(2)	N(3)–Fe(1)–O(1)	94.30(19)
N(2)–Fe(1)–O(2)	178.06(18)	N(3)–Fe(1)–O(2)	89.3(2)
N(2)–Fe(1)–O(1)	88.44(19)		

Table 3. Selected bond lengths (Å) and angles (°) for $[(L^{1})Fe^{III}(BA)](ClO_4)$ (**3^{ox}-ClO_4**).

Fe(1)–N(1)	1.960(16)	Fe(1)–N(2)	1.987(18)
Fe(1)–N(3)	1.971(16)	Fe(1)–C(6)	1.986(2)
Fe(1)–O(1)	1.928(14)	Fe(1)–O(2)	1.884(15)
C(25)–O(2)	1.288(2)	C(23)–O(1)	1.291(2)
C(23)–C(24)	1.402(3)	C(24)–C(25)	1.394(3)
C(6)–Fe(1)–N(1)	86.98(8)	C(6)–Fe(1)–O(1)	179.47(7)

N(1)–Fe(1)–N(2)	88.65(7)	C(6)–Fe(1)–N(3)	86.45(8)
O(1)–Fe(1)–O(2)	92.05(6)	N(2)–Fe(1)–N(3)	91.52(7)
C(6)–Fe(1)–N(2)	89.85(8)	N(3)–Fe(1)–N(1)	173.43(7)
N(1)–Fe(1)–O(1)	93.30(7)	N(1)–Fe(1)–O(2)	90.71(7)
O(2)–Fe(1)–C(6)	87.49(8)	N(3)–Fe(1)–O(1)	93.27(7)
N(2)–Fe(1)–O(2)	177.30(7)	N(3)–Fe(1)–O(2)	88.83(7)
N(2)–Fe(1)–O(1)	90.61(7)		

Graphical abstract

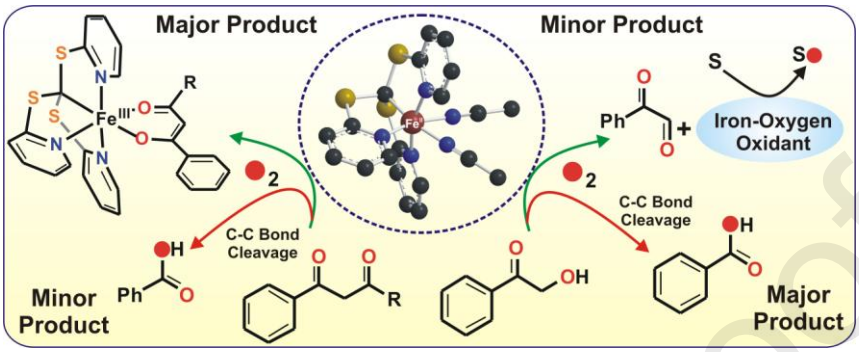

Ternary iron(II) complexes of a tripodal N3C ligand react with oxygen to display either metal center oxidation or aliphatic C-C bond cleavage depending upon the nature of co-ligand.

Highlights

- Three low-spin iron(II) complexes of an anionic N3C donor supporting ligand and β-diketones/α-hydroxy ketone co-ligands were prepared and characterized.
- All the complexes are reactive toward dioxygen in solution.
- The iron(II)-β-diketonate complexes primarily display metal-centric oxidation in the reaction with dioxygen.
- The iron(II)-α-hydroxy ketone complex undergoes oxidative C-C bond cleavage of the co-ligand.